nature chemical biology

ARTICLE

PUBLISHED ONLINE: 1 APRIL 2012 | DOI: 10.1038/NCHEMBIO.925

Reversible targeting of noncatalytic cysteines with chemically tuned electrophiles

Iana M Serafimova[1,2], Miles A Pufall[2,3,7], Shyam Krishnan[2,7], Katarzyna Duda[4], Michael S Cohen[1,2,5], Rebecca L Maglathlin[1,2], Jesse M McFarland[2], Rand M Miller[1,2], Morten Frödin[4] & Jack Taunton[1,2,6]*

Targeting noncatalytic cysteine residues with irreversible acrylamide-based inhibitors is a powerful approach for enhancing pharmacological potency and selectivity. Nevertheless, concerns about off-target modification motivate the development of reversible cysteine-targeting strategies. Here we show that electron-deficient olefins, including acrylamides, can be tuned to react with cysteine thiols in a rapidly reversible manner. Installation of a nitrile group increased the olefins' intrinsic reactivity, but, paradoxically, eliminated the formation of irreversible adducts. Incorporation of these electrophiles into a noncovalent kinase-recognition scaffold produced slowly dissociating, covalent inhibitors of the p90 ribosomal protein S6 kinase RSK2. A cocrystal structure revealed specific noncovalent interactions that stabilize the complex by positioning the electrophilic carbon near the targeted cysteine. Disruption of these interactions by protein unfolding or proteolysis promoted instantaneous cleavage of the covalent bond. Our results establish a chemistry-based framework for engineering sustained covalent inhibition without accumulating permanently modified proteins and peptides.

Cysteine shows rich chemistry through its nucleophilic thiol group. It is also one of the least common amino acids in proteins. Together, these properties make cysteine residues ideal for targeting with covalent drugs, which have the potential to show high levels of target specificity and a prolonged duration of action[1–3]. Although frequently designed to inactivate conserved, catalytically essential nucleophiles (for example, in serine, threonine and cysteine proteases), covalent inhibitors can achieve maximal selectivity among related targets by exploiting the intrinsic nucleophilicity of poorly conserved, noncatalytic cysteines[4]. This strategy, guided by structural bioinformatics analysis, has led to the design of selective, irreversible inhibitors of protein kinases[5–9] and, more recently, the NS3/4A serine protease from hepatitis C virus[10].

Protein kinases are challenging therapeutic targets from the standpoint of achieving sustained inhibition of the desired kinase without affecting structurally related kinases. Most of the 518 human kinases have an accessible noncatalytic cysteine within reach of the active site[11,12], and at least four cysteine-targeted kinase inhibitors are in clinical trials for advanced cancer indications. They all rely on an acrylamide electrophile to form an irreversible covalent bond with the kinase[4]. Acrylamide-based kinase inhibitors react irreversibly with glutathione[13] and may therefore react with proteins other than the desired target, especially proteins with hyper-reactive cysteines[14]. Although the risk may be low and more relevant to chronic diseases than to advanced cancer, there are currently no preclinical models that can accurately predict the toxicological potential of chemically reactive drugs and drug metabolites[15–17]. Thus, current drug-discovery efforts mostly aim to avoid the formation of irreversible covalent adducts.

With these considerations in mind, we sought reversible electrophilic inhibitors that would retain the advantages of covalent cysteine targeting (prolonged duration of action and high selectivity) without the potential liabilities associated with irreversible adduct formation. The few known covalent inhibitors that reversibly target noncatalytic cysteines were discovered by random high-throughput screening[18,19], and the chemical basis of their reversibility is not clear. In this study, we elucidate specific structural features that underlie reversible thiol addition to electron-deficient olefins, and we apply these principles to the design of reversible, cysteine-targeted kinase inhibitors.

RESULTS

Reversibility of thiol addition to activated olefins

Experiments in the 1960s revealed that, at physiological pH, simple thiols react instantaneously with 2-cyanoacrylates, but the products could not be isolated or structurally characterized[20]. A potential explanation for these results is that the reaction, possibly a Michael-type conjugate addition, is a rapid-equilibrium process. To test this hypothesis and define the structural requirements for rapid reversibility, we compared three simple Michael acceptors, activated by a methyl ester (**1**), a nitrile (**2**) or both electron-withdrawing groups (**3**) (**Fig. 1a**).

Reactions of acrylate **1** and acrylonitrile **2** with the model thiol, β-mercaptoethanol (βME), produced the stable thioether adducts **4** and **5**, which were easily isolated and characterized (**Supplementary Results**, **Supplementary Fig. 1**). By contrast, when we treated the doubly activated Michael acceptor **3** with βME (**Fig. 1a**), only the starting cyanoacrylate was recovered. Addition of increasing concentrations of βME caused a stepwise reduction in the prominent UV-visible absorption band of cyanoacrylate **3** (λ_{max} 304 nm), and fitting these titration data provided an apparent K_d of 9.4 mM (**Fig. 1b**). ^{1}H-NMR provided further spectroscopic evidence for the formation of an adduct corresponding to thioether **6**, and dilution experiments confirmed that the reaction was rapidly reversible (**Fig. 1c**). The facile reversion of thioether adduct **6** to the starting cyanoacrylate probably derives from its enhanced kinetic and

[1]Graduate Program in Chemistry and Chemical Biology, University of California–San Francisco, San Francisco, California, USA. [2]Department of Cellular and Molecular Pharmacology, University of California–San Francisco, San Francisco, California, USA. [3]Department of Biochemistry, Carver College of Medicine, University of Iowa, Iowa City, Iowa, USA. [4]Biotech Research & Innovation Centre and Centre for Epigenetics, University of Copenhagen, Denmark. [5]Weill Medical College, Cornell University, New York, New York, USA. [6]Howard Hughes Medical Institute, Chevy Chase, Maryland, USA. [7]These authors contributed equally to this work. *e-mail: taunton@cmp.ucsf.edu

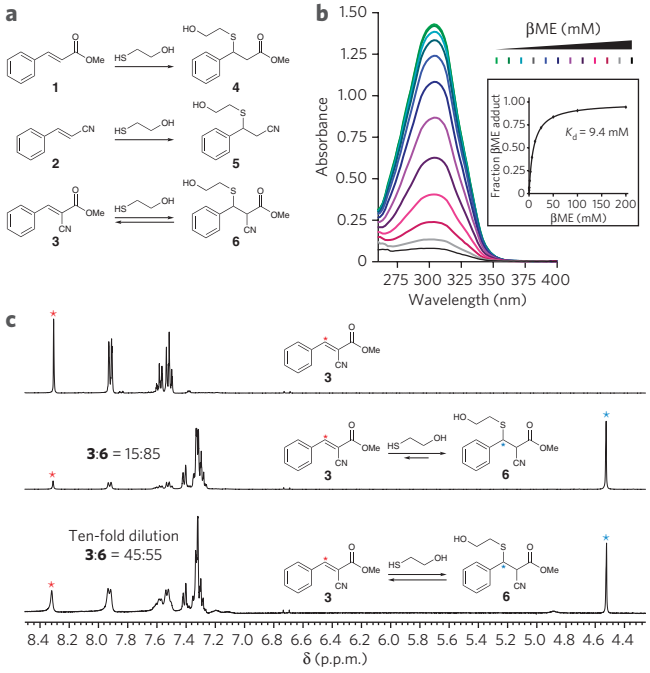

Figure 1 | Thiol reactivity of electron-deficient olefins. (**a**) Conjugate addition reactions of βME with olefins **1**–**3**. (**b**) Cyanoacrylate **3** (100 μM) was treated with increasing concentrations of βME and monitored by UV-visible absorption spectroscopy. The inset shows the fraction of βME adduct versus the concentration of βME, from which K_d was derived. (**c**) ^{1}H-NMR spectra showing reversible addition of βME to **3**. Cyanoacrylate **3** (90 mM, top spectrum) was treated with 100 mM βME in DMSO-d_6:PBS-d (3:1), affording an 15:85 mixture that favored the βME adduct **6** (middle). Upon ten-fold dilution, the equilibrium shifted to the left (bottom). Red and blue asterisks indicate protons used to determine ratios of **3**:**6**.

thermodynamic acidity, estimated to be 10–15 orders of magnitude greater than the carbon acidity of stable adducts **4** and **5** (ref. 21). Hence, the combined influence of a nitrile and an ester on the acidity of the αC-H bond facilitates rapid elimination of thiol adducts at physiological pH and at the same time accelerates the rate of thiol addition.

To test whether this chemistry is applicable to structurally related Michael acceptors, we synthesized five cyanoacrylamides with diverse substituents attached to the electrophilic β-carbon (**7**–**11**; **Supplementary Fig. 2**). We included entacapone, a cyanoacrylamide-based drug used for the treatment of Parkinson's disease; to our knowledge, the reactivity of entacapone toward thiols has not been reported previously. Similar to cyanoacrylate **3**, the cyanoacrylamides reacted with millimolar concentrations of βME in a manner that was reversed within seconds upon dilution (**Supplementary Fig. 2**). Depending on the β-substituent, K_d values ranged from 0.2 mM to 33 mM, corresponding to standard free energy changes (ΔG_o) of −2 kcal mol^{-1} to −5 kcal mol^{-1}. The ability of β-substituted cyanoacrylamide derivatives, including a widely used drug, to form rapidly reversible adducts with thiols suggested an attractive approach for targeting noncatalytic cysteines without the use of irreversible electrophiles.

Rational design of reversible covalent kinase inhibitors

We prepared a series of electrophilic pyrrolopyrimidines (**12**–**15**; **Fig. 2a**), analogous to the model Michael acceptors in **Figure 1**, and compared their biochemical activities against the C-terminal kinase domain (CTD) of the p90 ribosomal protein S6 kinase RSK2. The electrophilic β-carbon was designed to be proximal to Cys436 in the RSK2 active site on the basis of the predicted binding orientation of the pyrrolopyrimidine scaffold, similar to the irreversible fluoromethylketone-based inhibitor (referred to as FMK; see **Supplementary Figure 4** for structure) developed previously[6,22]. Treatment of the RSK2-CTD with five equivalents of acrylate (**12**) or acrylonitrile (**13**) led to the slow formation of a covalent adduct, as revealed by LC/MS (**Fig. 2a**). By contrast, the doubly activated Michael acceptors cyanoacrylate (**14**) and cyanoacrylamide (**15**) failed to produce adducts detectable by LC/MS (**Fig. 2a**), despite being more than 200-fold more potent than the singly activated Michael acceptors **12** and **13** in kinase activity assays (**Fig. 2b**). Mutation of Cys436 to valine conferred ~1,000-fold resistance to inhibitors **14** and **15** (**Supplementary Fig. 3**), suggesting that potent RSK2 inhibition requires covalent bond formation. Cyanoacrylamide **15** reacted rapidly and reversibly with βME and glutathione (K_d = 5.1 mM and 7.3 mM, respectively), but pretreatment with 10 mM glutathione had no effect on its ability to inhibit RSK2 (half-maximum inhibitory concentration (IC_{50}) = 4 nM; **Supplementary Fig. 3**). Cyanoacrylamide **15** did not react substantially with lysine or ethanolamine (up to 100 mM; **Supplementary Fig. 3**).

RSK2-CTD kinase activity recovered from inhibition by **14** after dialysis for 3 d at 4 °C, whereas recovery from **15** was much slower under these conditions (**Fig. 2c**). To estimate their biochemical dissociation rates, we developed a kinetic trapping assay in which RSK2-CTD was first saturated with a reversible inhibitor, followed by treatment with a large excess of FMK. In the absence of inhibitor pretreatment, FMK (100 μM) reacted with Cys436 of RSK2-CTD to form a 1:1 covalent adduct ($t_{1/2}$ < 1 min), as determined by MS analysis (**Supplementary Fig. 4**). Pretreatment of RSK2-CTD (5 μM) with **14** or **15** (10 μM) caused a strong reduction in the rate of FMK labeling (**Fig. 2d**), from which we could estimate dissociation half-times of 42 min and 245 min, respectively. Thus, inhibition of RSK2-CTD by **15** is long-lived but fully reversible, with complete dissociation occurring on a timescale of several hours.

We selected the *N*-isopropyl cyanoacrylamide **15** (hereafter referred to as CN-NHiPr) for further biochemical and cellular experiments because of its greater potency and slower off-rate compared to **14**. Kinase profiling[23] showed that CN-NHiPr is highly selective for the C-terminal kinase domains of RSK1 and RSK4 (RSK2-CTD was not on the panel of profiled kinases). Aside from RSK1-CTD and RSK4-CTD, only 6 of the 442 kinases profiled showed >70% inhibition by 1 μM CN-NHiPr relative to the DMSO control (**Supplementary Table 1**). Subsequent K_d determinations showed that CN-NHiPr bound RSK1-CTD (K_d = 540 pM) with an affinity ~80-fold higher than that of MAP3K1 and at least 400-fold higher than the affinities of the remaining five kinases (STK16, RIPK2, RET, MEK5 and PDGFRB) (**Supplementary Fig. 5**).

Sustained, quasi-irreversible occupancy of RSK in cells

We compared the cellular activity of CN-NHiPr with that of FMK, which has previously been shown to be an irreversible inhibitor of endogenous RSK1 and RSK2 (refs. 6,22). Treatment of MDA-MB-231 breast cancer cells with CN-NHiPr for 2 h led to potent inhibition of RSK2-CTD–mediated autophosphorylation of Ser386 (half-maximal effective concentration (EC_{50}) < 10 nM, **Fig. 3a**), a key regulatory site for the N-terminal effector kinase domain[24]. With a similar dose response, CN-NHiPr prevented an irreversible fluorescent probe, FMK-BODIPY[22], from labeling RSK1 and RSK2 in cells (**Fig. 3b**). Despite its irreversible binding mode, FMK was less potent than CN-NHiPr in both the cellular occupancy and autophosphorylation assays, suggesting that CN-NHiPr enters cells and binds endogenous RSK1 and RSK2 with faster kinetics. Washout experiments showed that the duration of RSK1 and RSK2 occupancy by CN-NHiPr was, notably, indistinguishable from that of FMK. After washout of FMK or CN-NHiPr, reappearance of inhibitor-free RSK1 and RSK2 required at least 48 h, presumably the

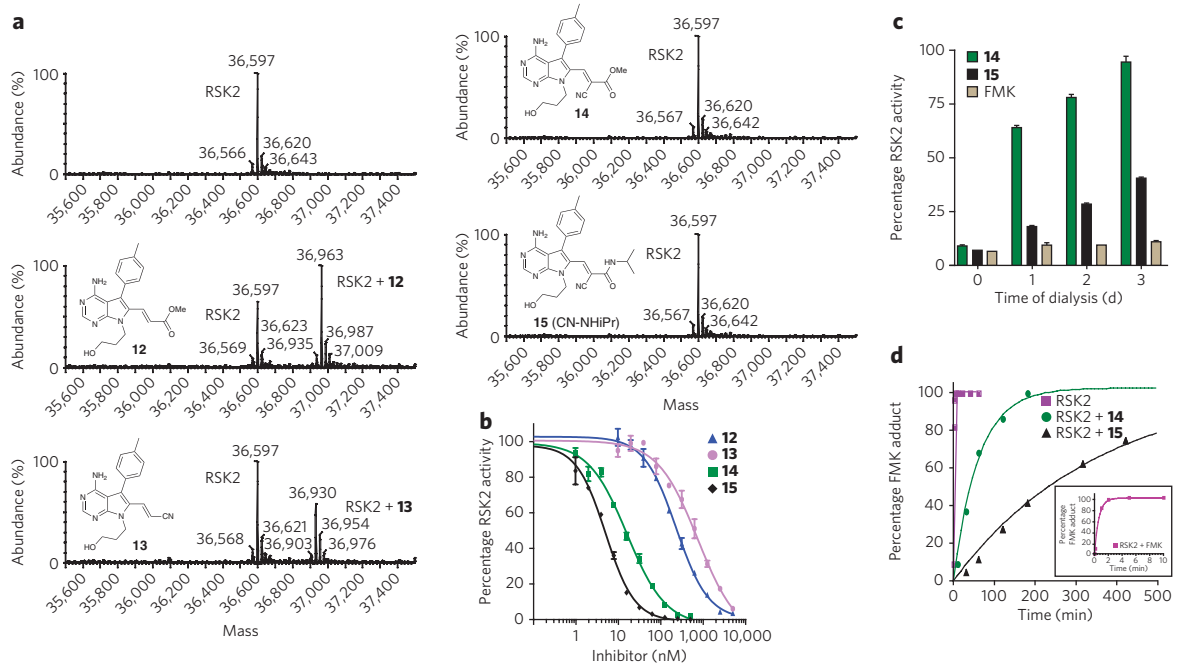

Figure 2 | Sustained, reversible inhibition of RSK2-CTD by doubly activated Michael acceptors. (**a**) RSK2-CTD (5 μM) was treated with pyrrolopyrimidines **12**–**15** (25 μM) for 1 h, followed by LC/MS analysis. Observed molecular masses of unmodified RSK2-CTD and the 1:1 adducts with **12** and **13** are consistent with the predicted values. (**b**) *In vitro* kinase assays of RSK2-CTD. Shown are mean values from duplicate measurements (± range). Data were fit with PRISM 4.0 to provide IC_{50} values (**Supplementary Fig. 3a**). (**c**) RSK2-CTD (50 nM) was treated with the indicated inhibitors (1 μM) or DMSO for 1 h at room temperature, before dialyzing at 4 °C. Aliquots were tested daily for kinase activity and normalized to a DMSO control (mean ± s.d., from three experiments). (**d**) RSK2-CTD (5 μM) was pretreated with inhibitors **14** or **15** (10 μM) for 1 h, followed by addition of excess FMK (100 μM final). At each time point, an aliquot was removed and quenched by diluting 1:1 into 0.4% (v/v) formic acid. Relative amounts of RSK2-CTD and the FMK adduct were quantified by LC/MS. Progress curve fits to a single exponential were used to estimate the dissociation half-times of **14** and **15**. Inset, progress curve detail showing reaction of RSK2-CTD with 100 μM FMK.

time required for RSK1 and RSK2 resynthesis (**Fig. 3c**). Similar to FMK, CN-NHiPr abolished RAF-induced epithelial cell migration and invasion (**Fig. 3d–f**), consistent with the recently established role of RSK signaling in these processes[25–27].

Cocrystal structure of the RSK2-cyanoacrylate complex

A cocrystal structure provided insight into the molecular basis of sustained RSK2 inhibition by doubly activated Michael acceptors (**Fig. 4a**). We screened several related cyanoacrylate and cyanoacrylamide inhibitors and obtained the best diffraction data (2.4-Å resolution) with a *tert*-butyl cyanoacrylate derivative (**16**; **Supplementary Fig. 3a**) that has similar potency and dissociation kinetics ($t_{1/2}$ = 163 min) to CN-NHiPr. The structure confirms the covalent nature of the complex (Protein Data Bank (PDB) code 4D9U; **Fig. 4a**), with strong electron density connecting Cys436 to the electrophilic β-carbon of the cyanoacrylate (**Supplementary Fig. 6a**). A second cysteine (Cys560) within ~7 Å of the electrophilic carbon is incapable of forming a stable covalent bond, as indicated by the ~1,000-fold decrease in potency of CN-NHiPr toward C436V RSK2 (**Supplementary Fig. 3**). Hydrogen bonds between the pyrrolopyrimidine scaffold, the RSK2 hinge region and the side chain of Thr493 position the electrophilic β-carbon beneath Cys436 and are probably essential for driving covalent bond formation (**Fig. 4a**). An additional anchor is provided by the *p*-tolyl group, which packs against the gatekeeper side chain (Thr493) and extends into a hydrophobic pocket. Mutation of Thr493 to methionine in RSK2-CTD conferred ~1,000-fold resistance to CN-NHiPr (**Supplementary Fig. 6b**). RSK3-CTD and the related kinase domains of MSK1/2 have a methionine gatekeeper, explaining their insensitivity to CN-NHiPr (**Supplementary Table 1**).

Protein unfolding promotes covalent bond dissociation

If the combined nonbonded interactions between RSK2 and the pyrrolopyrimidine are essential for stabilizing the covalent bond, disruption of the kinase domain's tertiary fold should promote rapid elimination of Cys436 and regeneration of the original Michael acceptor. We tested this hypothesis by monitoring covalent bond formation in solution with UV-visible spectroscopy. Treatment of CN-NHiPr (20 μM in pH 7.5 buffer) with a slight excess of RSK2-CTD (25 μM) caused disappearance of the strong 400-nm absorption peak (**Fig. 4b**,**c**), consistent with nucleophilic attack on the cyanoacrylamide. Mutation of Cys436 abolished this effect (**Fig. 4c**), showing that none of the remaining cysteines (including Cys560 in the ATP-binding site) detectably reacts with CN-NHiPr, even at millimolar concentrations (**Supplementary Fig. 7**). When the covalent RSK2-CTD–CN-NHiPr complex was unfolded by the addition of SDS or guanidine, the cyanoacrylamide absorption peak reappeared within seconds (**Fig. 4b**,**c**), and LC/MS analysis indicated quantitative recovery of CN-NHiPr (**Supplementary Fig. 7**). Proteolytic digestion of the complex with trypsin or proteinase K also promoted complete reversal of the covalent bond (**Fig. 4c**), suggesting that cyanoacrylamide-modified peptides derived from cellular RSK turnover would be short-lived.

We have shown that cyanoacrylamides react reversibly with model thiols and recombinant RSK2-CTD. However, formation of irreversible adducts with endogenous full-length RSK or other cellular proteins remained possible, especially given the apparent irreversible binding to RSK1 and RSK2 (resistant to washout) in cells (**Fig. 3c**). We addressed this possibility by treating cells with fluorescent BODIPY conjugates derived from FMK, CN-NHiPr and the pyrrolopyrimidine scaffold as a nonelectrophilic control (see **Supplementary Fig. 8** for chemical structures). Analysis of cell

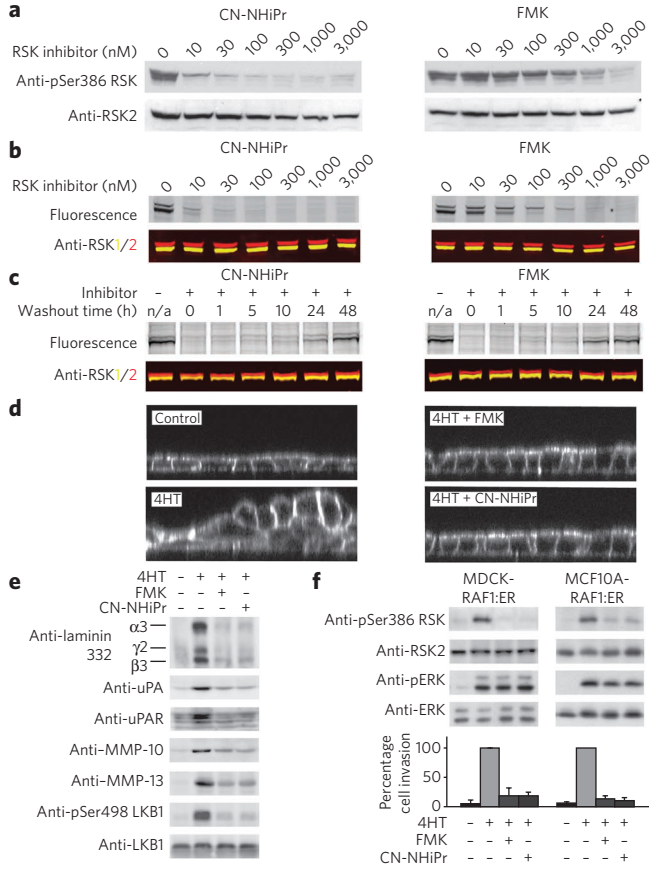

Figure 3 | Sustained inhibition of cellular RSK1 and RSK2 by CN-NHiPr. (**a**) MDA-MB-231 cells were treated with CN-NHiPr or FMK. Cell lysates were immunoblotted with antibodies for pSer386 RSK (Anti-pSer386 RSK) or RSK2 (Anti-RSK2). (**b**) MDA-MB-231 cells were treated with CN-NHiPr or FMK, followed by FMK-BODIPY (3 μM). Cell lysates were resolved by SDS-PAGE and detected by in-gel fluorescence scanning or immunoblotting with antibodies for RSK1 (yellow) and RSK2 (red) (Anti-RSK1/2). (**c**) MDA-MB-231 cells were treated with CN-NHiPr or FMK (1 μM). The medium was exchanged and cells were harvested at the indicated times after inhibitor washout. Cell lysates were treated with FMK-BODIPY (5 μM). Proteins were resolved on SDS-PAGE and detected by in-gel fluorescence or immunoblotting for RSK1 (yellow) and RSK2 (red). (**d**) Polarized MDCK-RAF:ER cell monolayers were treated with CN-NHiPr or FMK (2 μM) and stimulated with 4HT (1 μM) to activate RAF-dependent epithelial cell multilayering. After 24 h, cells were imaged by confocal fluorescence microscopy (*xz* plane). (**e**) Polarized MDCK-RAF:ER cell monolayers were treated as in **d**. After 24 h, cell lysates and conditioned medium were analyzed by immunoblotting for the indicated proteins. Laminin 332 designates a specific form of laminin comprising α3, γ2 and β3 subunits. uPA, urokinase-type plasminogen activator; uPAR, uPA receptor; LKB1, liver kinase B1. (**f**) MDCK-RAF:ER and MCF10A-RAF:ER cells were treated with CN-NHiPr or FMK (2 μM) and 4HT (1 μM) as indicated. Cells were then either lysed for immunoblot analysis or trypsinized and subjected to Matrigel invasion assays. After 24 h, cell invasion was quantified and expressed as a percentage of the maximum value (mean ± s.d. from three experiments).

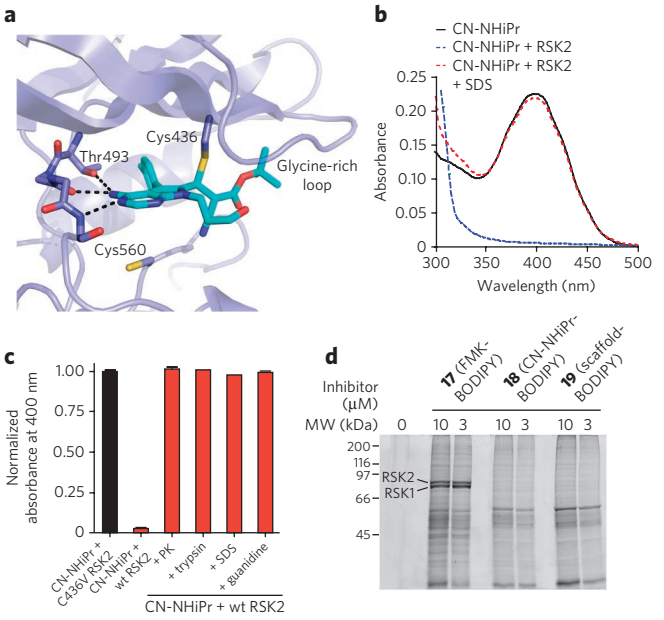

Figure 4 | Specific noncovalent interactions drive covalent bond formation. (**a**) Cocrystal structure of RSK2-CTD bound to *tert*-butyl cyanoacrylate (**16**). Ribbon representation of RSK2-CTD with **16** in cyan highlights hydrogen bonds to the hinge and the gatekeeper, Thr493. Note the close proximity of Cys560, which does not form a covalent bond with the electrophilic β-carbon. (**b**) UV-visible spectra of CN-NHiPr showing the 400-nm cyanoacrylamide absorption peak. CN-NHiPr (20 μM, black curve) was treated with wild-type RSK2-CTD (25 μM), resulting in a loss of the cyanoacrylamide peak (blue curve). Addition of SDS (2% (w/v) final) caused instantaneous recovery of the cyanoacrylamide (red curve). (**c**) Effect of protein unfolding (2% (w/v) SDS; 3 M guanidine HCl) and proteolysis (proteinase K (PK), trypsin) on the covalent complex derived from CN-NHiPr (20 μM) and RSK2-CTD (25 μM). Recovery of free CN-NHiPr was determined by quantifying the absorbance at 400 nm (mean ± s.d. from three experiments). C436V RSK2-CTD (25 μM) had no effect on the CN-NHiPr absorption peak. (**d**) Modification of cellular proteins by BODIPY conjugates of FMK (**17**), CN-NHiPr (**18**) and the pyrrolopyrimidine scaffold (**19**) (see **Supplementary Fig. 8** for structures). MDA-MB-231 cells were treated with the indicated BODIPY conjugates. Cell lysates were resolved by SDS-PAGE, and BODIPY adducts were detected by in-gel fluorescence scanning.

lysates by SDS-PAGE revealed several prominent bands labeled by the irreversible probe FMK-BODIPY, including endogenous RSK1 and RSK2 (ref. 22; **Fig. 4d**). By contrast, BODIPY conjugates of CN-NHiPr and the nonelectrophilic scaffold failed to label RSK1 and RSK2. Instead, both BODIPY conjugates bound weakly to an identical subset of denatured proteins, presumably in a noncovalent manner. We conclude that specific interactions provided by the folded kinase domain, together with a precisely positioned cysteine, are required to cooperatively stabilize a covalent complex with CN-NHiPr. The lack of irreversible adduct formation by CN-NHiPr is counterintuitive given that it is more than 50,000 times more reactive toward thiols than is FMK (reaction with 10 mM glutathione: CN-NHiPr $t_{1/2}$ < 1 s; FMK $t_{1/2}$ = 16 h).

DISCUSSION

In this study, we report a new approach for targeting noncatalytic cysteines with reversible covalent inhibitors. The predominant strategy for targeting noncatalytic cysteines, exemplified by several acrylamide-based kinase inhibitors in clinical trials, has been to minimize the intrinsic chemical reactivity of the electrophile as much as possible[4]. This strategy derives from the chemically intuitive hypothesis that attenuated electrophiles have a reduced likelihood of reacting irreversibly with off-target proteins. Our results challenge this notion. Although attenuated Michael acceptors such as acrylamides may react slowly with most cysteine residues, the probability of modifying a hyper-reactive cysteine (comprising up to ~10% of solvent-exposed cysteines[14]) is unpredictable; such off-target reactions are clearly undesirable.

Our chemical and biochemical experiments show that addition of a nitrile group (with a molecular mass of only 26 Da) converts irreversible Michael acceptors (for example, acrylate or acrylamide) into electrophiles with unanticipated properties. The resulting electrophiles (for example, cyanoacrylate or cyanoacrylamide) react with cysteine thiols under physiological conditions in a manner that is energetically favorable yet rapidly reversible, thus minimizing the chance of producing irreversibly modified peptides. Adding the nitrile group to the α-carbon of an acrylamide increases the susceptibility of the β-carbon to nucleophilic attack but also stabilizes the resultant carbanion. This leads to a kinetic regime in which thiol addition and elimination proceed on a subsecond-to-second time scale, an unexpected result that, to our knowledge, has not been demonstrated previously. Rapid thiol-addition and thiol-elimination chemistry seems to be a general property of cyanoacrylamides and, in preliminary work, extends to some, but not all, combinations of two electron-withdrawing groups in doubly activated Michael acceptors. We envision that the reversible covalent targeting strategy described herein can be applied to any kinase that has an exposed cysteine within striking distance of the active site, provided that the geometric requirements for covalent bond formation are satisfied with minimal strain. More generally, by using structural bioinformatics to identify solvent-exposed cysteines near potential small-molecule–binding sites, it may be possible to apply this strategy to additional target classes outside of the protein kinase family.

METHODS

Chemicals. The following chemicals were commercially obtained and used without further purification: methyl *trans*-cinnamate (**1**), 99% pure, Sigma-Aldrich; cinnamonitrile (**2**), 97% pure, Sigma-Aldrich; entacapone, 99% pure, AK Scientific; phorbol 12-myristate 13-acetate, >99% pure, Sigma-Aldrich; and (*Z*)-4-hydroxytamoxifen (4HT), >97% pure, Calbiochem.

Inhibitors. Compounds **3**–**16** and BODIPY conjugates **17**–**19** were synthesized and characterized as described in the **Supplementary Methods**. FMK was synthesized as described[6], and the characterization and purity matched published standards.

Protein purification. RSK2-CTD was expressed and purified as described[28]. Briefly, wild-type and mutant RSK2-CTDs were expressed in *Escherichia coli* from pET-46 EK/LIK His_6 fusion vectors and purified by Ni-NTA affinity chromatography in a 50 mM Tris (pH 8.0), 0.5 M NaCl and 10–500 mM imidazole gradient, followed by cleavage of the His_6 tag and a second purification with an S75 size-exclusion column.

Protein kinase activity assays. RSK2-CTD was assayed for kinase activity as described[6,22]. Detailed methods describing the determination of inhibitor IC_{50} values for RSK2-CTD, as well as kinase activity recovery after inhibitor dialysis, are provided in the **Supplementary Methods**.

Covalent modification of RSK2-CTD. LC/MS was used to detect covalent adducts between the various pyrrolopyrimidine electrophilic derivatives and RSK2-CTD. Purified RSK2-CTD (5 μM) was incubated with the various inhibitors (25 μM) for 1 h at 20–25 °C and was analyzed by liquid chromatography and in-line ESI mass spectrometry as described in the **Supplementary Methods**.

UV-visible spectroscopic assays. Detailed methods for determining the dissociation constants of electrophile and thiol adducts are provided in the **Supplementary Methods**. Briefly, electrophilic compounds (100–200 μM in PBS (pH 7.4)) were treated with increasing concentrations of βME or glutathione before acquiring absorption spectra. The extent of electrophile consumption was determined by monitoring the disappearance of the absorbance at λ_{max}.

Cellular assays. Cellular RSK inhibition and occupancy using FMK-BODIPY was determined as described[22]. MDA-MB231 cells (ATCC) were grown until confluence in the presence of DMEM supplemented with 10% (v/v) FBS. Before inhibitor treatment, the medium was exchanged to serum-free DMEM, and the cells were treated for 2 h with the various inhibitors and then lysed and analyzed by various methods as described in the **Supplementary Methods**. Multilayering and Matrigel invasion assays using MDCK-RAF:ER cells, which stably express tamoxifen-activatable RAF1 fused to the ligand-binding domain of the estrogen receptor, were performed as described[25].

Crystal structure determination and refinement. Cocrystals of **16** bound to RSK2-CTD were obtained in 0.1 M Tris (pH 8.5), 25% (w/v) PEG 3350 (PDB 4D9U). Details about data collection, structure determination and refinement are described in the **Supplementary Methods**. Briefly, purified RSK2-CTD was concentrated to between 5 mg ml^{-1} and 10 mg ml^{-1} in buffer (20 mM Tris (pH 8.0), 50 mM NaCl and 1 mM DTT) and incubated with one molar equivalent of **16**. Hanging drops of 1 μl of this mixture and 1 μl precipitant solution (0.1 M Tris (pH 8.5), 25% (w/v) PEG 3350) were used to obtain crystals. Crystals were cryoprotected in mother liquor with 30% (v/v) ethylene glycol and flash frozen in liquid nitrogen before crystallographic data acquisition. The data sets were processed using XDS (http://xds.mpimf-heidelberg.mpg.de/), and the structure was solved by molecular replacement.

Received 11 August 2011; accepted 2 February 2012; published online 1 April 2012

References

1. Copeland, R.A., Pompliano, D.L. & Meek, T.D. Opinion — Drug-target residence time and its implications for lead optimization. *Nat. Rev. Drug Discov.* **5**, 730–739 (2006).
2. Potashman, M.H. & Duggan, M.E. Covalent modifiers: an orthogonal approach to drug design. *J. Med. Chem.* **52**, 1231–1246 (2009).
3. Smith, A.J.T., Zhang, X.Y., Leach, A.G. & Houk, K.N. Beyond picomolar affinities: quantitative aspects of noncovalent and covalent binding of drugs to proteins. *J. Med. Chem.* **52**, 225–233 (2009).
4. Singh, J., Petter, R.C., Baillie, T.A. & Whitty, A. The resurgence of covalent drugs. *Nat. Rev. Drug Discov.* **10**, 307–317 (2011).
5. Fry, D.W. *et al.* Specific, irreversible inactivation of the epidermal growth factor receptor and erbB2, by a new class of tyrosine kinase inhibitor. *Proc. Natl. Acad. Sci. USA* **95**, 12022–12027 (1998).
6. Cohen, M.S., Zhang, C., Shokat, K.M. & Taunton, J. Structural bioinformatics-based design of selective, irreversible kinase inhibitors. *Science* **308**, 1318–1321 (2005).
7. Honigberg, L.A. *et al.* The Bruton tyrosine kinase inhibitor PCI-32765 blocks B-cell activation and is efficacious in models of autoimmune disease and B-cell malignancy. *Proc. Natl. Acad. Sci. USA* **107**, 13075–13080 (2010).
8. Zhou, W. *et al.* Novel mutant-selective EGFR kinase inhibitors against EGFR T790M. *Nature* **462**, 1070–1074 (2009).
9. Zhou, W. *et al.* A structure-guided approach to creating covalent FGFR inhibitors. *Chem. Biol.* **17**, 285–295 (2010).
10. Hagel, M. *et al.* Selective irreversible inhibition of a protease by targeting a noncatalytic cysteine. *Nat. Chem. Biol.* **7**, 22–24 (2011).
11. Leproult, E., Barluenga, S., Moras, D., Wurtz, J.M. & Winssinger, N. Cysteine mapping in conformationally distinct kinase nucleotide binding sites: application to the design of selective covalent inhibitors. *J. Med. Chem.* **54**, 1347–1355 (2011).
12. Zhang, J., Yang, P.L. & Gray, N.S. Targeting cancer with small molecule kinase inhibitors. *Nat. Rev. Cancer* **9**, 28–39 (2009).
13. Wissner, A. *et al.* Synthesis and structure-activity relationships of 6,7-disubstituted 4-anilinoquinoline-3-carbonitriles. The design of an orally active, irreversible inhibitor of the tyrosine kinase activity of the epidermal growth factor receptor (EGFR) and the human epidermal growth factor receptor-2 (HER-2). *J. Med. Chem.* **46**, 49–63 (2003).
14. Weerapana, E. *et al.* Quantitative reactivity profiling predicts functional cysteines in proteomes. *Nature* **468**, 790–795 (2010).
15. Uetrecht, J. Idiosyncratic drug reactions: past, present, and future. *Chem. Res. Toxicol.* **21**, 84–92 (2008).
16. Evans, D.C., Watt, A.P., Nicoll-Griffith, D.A. & Baillie, T.A. Drug-protein adducts: an industry perspective on minimizing the potential for drug bioactivation in drug discovery and development. *Chem. Res. Toxicol.* **17**, 3–16 (2004).
17. Park, B.K. *et al.* Managing the challenge of chemically reactive metabolites in drug development. *Nat. Rev. Drug Discov.* **10**, 292–306 (2011).
18. Lee, G. *et al.* Novel inhibitors of hepatitis C virus RNA-dependent RNA polymerases. *J. Mol. Biol.* **357**, 1051–1057 (2006).
19. Patch, R.J. *et al.* Identification of diaryl ether-based ligands for estrogen-related receptor α potential antidiabetic agents. *J. Med. Chem.* **54**, 788–808 (2011).
20. Pritchard, R.B., Lough, C.E., Currie, D.J. & Holmes, H.L. Equilibrium reactions of N-butanethiol with some conjugated heteroenoid compounds. *Can. J. Chem.* **46**, 775–781 (1968).
21. Pearson, R.G. & Dillon, R.L. Rates of ionization of pseudo acids. IV. Relation between rates and equilibria. *J. Am. Chem. Soc.* **75**, 2439–2443 (1953).
22. Cohen, M.S., Hadjivassiliou, H. & Taunton, J. A clickable inhibitor reveals context-dependent autoactivation of p90 RSK. *Nat. Chem. Biol.* **3**, 156–160 (2007).
23. Fabian, M.A. *et al.* A small molecule–kinase interaction map for clinical kinase inhibitors. *Nat. Biotechnol.* **23**, 329–336 (2005).
24. Frödin, M. & Gammeltoft, S. Role and regulation of 90 kDa ribosomal S6 kinase (RSK) in signal transduction. *Mol. Cell. Endocrinol.* **151**, 65–77 (1999).

25. Doehn, U. *et al.* RSK Is a principal effector of the RAS-ERK pathway for eliciting a coordinate promotile/invasive gene program and phenotype in epithelial cells. *Mol. Cell* **35**, 511–522 (2009).
26. Kang, S. *et al.* p90 ribosomal S6 kinase 2 promotes invasion and metastasis of human head and neck squamous cell carcinoma cells. *J. Clin. Invest.* **120**, 1165–1177 (2010).
27. Smolen, G.A. *et al.* A genome-wide RNAi screen identifies multiple RSK-dependent regulators of cell migration. *Genes Dev.* **24**, 2654–2665 (2010).
28. Malakhova, M. *et al.* Structural basis for activation of the autoinhibitory C-terminal kinase domain of p90 RSK2. *Nat. Struct. Mol. Biol.* **15**, 112–113 (2008).

Acknowledgments

We thank D. King (Howard Hughes Medical Institute Mass Spectrometry Laboratory) for protein mass spectrometry expertise, members of the Taunton laboratory for insight, and the staff of Advanced Light Source (ALS) Beamline 8.3.1 for help with data collection. This work was supported by grants from the US National Institutes of Health (NIH) (GM071434 to J.T., CA020535 and K99CA149088 to M.A.P., F32GM087052 to J.M.M.), the Leukemia and Lymphoma Society (5416-7 to M.A.P.), and the California Tobacco Related Disease Research Program (19FT-0091 to S.K.). We acknowledge the University of California San Francisco (UCSF) Mass Spectrometry Facility (supported by NIH grant P41RR001614).

Author contributions

J.T. conceived of and directed the study. I.M.S., S.K., M.S.C., R.L.M., J.M.M. and R.M.M. synthesized compounds, designed and executed chemical, biochemical and cellular experiments, and analyzed data. K.D. and M.F. designed and executed the cellular multilayering and invasion experiments. M.A.P. solved and refined the cocrystal structure. J.T., I.M.S. and S.K. wrote the manuscript with contributions from all other authors.

Competing financial interests

The authors declare competing financial interests: details accompany the full-text HTML version of the paper at http://www.nature.com/naturechemicalbiology/.

Additional information

Supplementary information and chemical compound information is available online at http://www.nature.com/naturechemicalbiology/. Reprints and permissions information is available online at http://www.nature.com/reprints/index.html. Correspondence and requests for materials should be addressed to J.T.